Civil Engineering
Engenharia Civil

The effect of concentrated transversal force on the moment resistance of rectangular hollow steel section beams

http://dx.doi.org/10.1590/0370-44672018720121

Jacqueline Maria Flor[1,2]
https://orcid.org/0000-0001-8209-4503
Ricardo Hallal Fakury[1,3]
https://orcid.org/0000-0002-1884-5699
Rodrigo Barreto Caldas[1,4]
https://orcid.org/0000-0002-0851-7632
Davi Pedrosa de Aguiar[1,5]
https://orcid.org/0000-0003-2286-5841

[1]Universidade Federal de Minas Gerais – UFMG,
Escola de Engenharia, Departamento de
Engenharia de Estruturas,
Belo Horizonte - Minas Gerais – Brasil.

E-mails: [2]flor@dees.ufmg.br, [3]fakury@dees.ufmg.br,
[4]caldas@dees.ufmg.br, [5]daviaguiar@outlook.com

Abstract

This article reports on a preliminary investigation about the effect of concentrated transversal force on the bending moment resistance of rectangular hollow steel section (RHS) beams. Two six-meter-long specimens with yield strength of 300 MPa and cross-section size of 250×150×6.4 mm were subjected to bending tests using a four-point load configuration. A three-dimensional nonlinear finite element model was developed by using the software ABAQUS to simulate the flexural behavior of the RHS beams. The model was validated against the experimental results and subsequently used to conduct a parametric study. The investigated parameters were the force application method and the corner radius between the webs and the flanges of the rectangular tube. The results showed that RHS beams may undergo failure due to large localized plastic deformations beneath the concentrated force, whenever this force causes compression on the webs. The use of a doubler plate on both webs can significantly reduce the detrimental effect on the bending moment resistance. Moreover, the effect is shown to be more pronounced for rectangular hollow steel sections with larger corner radius.

Keywords: rectangular hollow steel section beam; effect of concentrated force; doubler plate; bending moment resistance.

1. Introduction

Rectangular hollow steel section (RHS) beams are often employed in floor and roof structures mainly due to architectural advantages compared to open section steel profiles, providing to the building a clean and pleasantly aesthetic appearance (Araújo *et al.*, 2016). The ease of the connections to flat surfaces gives rectangular tubes constructive advantages over circular tubes.

In general, the bending moment resistance of RHS beams, like other steel beams with different cross-sectional shapes, is limited by the occurrence of lateral-torsional buckling (LTB), local buckling of the compression flange (FLB), local buckling of both webs (WLB), and failure due to the concentrated transversal loading on the profile flange, also referred to as patch loading. The Brazilian standard ABNT NBR 8800: 2008 establishes limiting values for the beam cross-section slenderness parameters for the compression flange and for the webs that govern the determination of the bending moment resistance for the LTB, FLB and WLB ultimate limit states. No consideration is given to failure by concentrated transversal force. Furthermore, no reference in literature on this subject has been found by the authors.

On the other hand, for I sections, there are provisions for the failure modes of a member subjected to a concentrated transversal force when it acts on a flange, causing either compression or tension to the webs. When the required strength is exceeded by the loading condition, transversal stiffeners and/or doubler plates shall be provided and sized for the difference between the required and available strength. Several researchers have dealt with this subject, such as Sherbourne and Jensen (1957), Graham *et al.* (1959, 1960), Roberts (1981), Summers and Yura (1982), Elgaaly (1983), Elgaaly and Salkar (1991), Carter (1999), Troup (1999), Prochnow *et al.* (2000), and Hajjar *et al.* (2003).

According to ABNT NBR 8800: 2008, RHS beams are not subjected to LTB, FLB and WLB when the slenderness parameter, λ, corresponding to each of these ultimate limit states, does not exceed the limit slenderness parameter for plastic design λ_p. In this case, the collapse of the beam will occur due to the yielding of the entire cross-section (formation of plastic hinge) and, consequently, the bending moment resistance (M_{Rk}) will be the plastic moment (M_{pl}). Table 1 presents the slenderness parameters λ e λ_p for LTB, FLB and WLB ultimate limit states. In this table, b denotes the width of the straight portion of the flanges, h denotes the depth of the straight portion of the webs, t denotes the wall-thickness, A is the cross-sectional area, J is the torsional constant, r_y is the

radius of gyration about the y-axis perpendicular to the bending x-axis, and L_b is the laterally unbraced length of the beam. As for the variables related to the properties of steel, E is the modulus of elasticity and f_y is the yield strength.

Ultimate Limit State	λ	λ_p
LTB	L_b / r_y	$0.13E\sqrt{JA} / M_{pl}$
FLB	b / t	$1.12\sqrt{E / f_y}$
WLB	h / t	$2.42\sqrt{E / f_y}$

Table 1
Slenderness parameters λ and λ_p.

This study aims to do a preliminary investigation on the effect of concentrated transversal forces on the bending moment resistance of RHS beams, limited to the following scope: (*a*) simply supported beams subjected to four-point bending due to concentrated transversal forces with a shear span equal to one third of the clear span; (*b*) cross-section slenderness parameter λ not superior to λ_p for LTB, FLB and WLB; and (*c*) concentrated transversal forces applied to the RHS beam in two different ways: (*i*) directly applied to the flat portion of the upper flange; and (*ii*) similarly, but with doubler plates welded on the straight portion of the webs.

In order to achieve this objective, the study comprised the following phases. First, bending tests were conducted on fullscale RHS beam specimens at the laboratory; second, Finite Element Method (FEM), for which a numerical model was developed to simulate the behavior of the RHS beam specimens; third, the FEM model was used to investigate the two different modes of application of the concentrated forces to the RHS beams; forth, numerical results for the bending moment resistance were compared to the predicted values for the cross-section plastic moment.

Additionally, the numerical analysis also investigated the influence of the outer r_o and inner r_i corner radius (Figure 1) between the flanges and the webs of the RHS steel profile on the bending moment resistance.

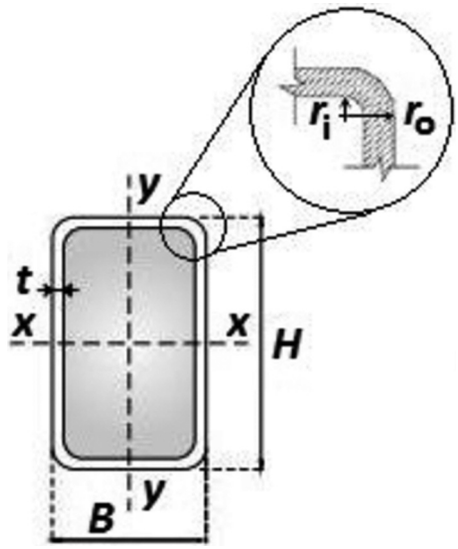

Figure 1
Specimen dimensions.

2. Experimental tests: materials and methods

Two rectangular steel tubes with characteristic yield strength of 300 MPa and cross-sectional nominal dimensions of 250 mm in depth (*H*), 150 mm in width (*B*) and 6.4 mm in wall thickness (*t*), as shown in Figure 1, were employed in the experimental study. The rectangular tubular profiles manufactured by Vallourec are produced from the cold forming of hot rolled circular tubular profiles. Hot rolling consists of the drilling, under high temperatures, of a billet in a punch mill. Due to the very high amount of cold working during the forming process, particularly in the corners of thick-walled square and rectangular hollow steel sections, the rectangular tubes produced by Vallourec are subjected to a post-production heat treatment at 450°C or higher and outdoor cooling afterwards to provide stress relief throughout the cross section. Steel tube cross-sectional real dimensions were measured at both ends of each RHS specimen prior to the test as follows: (a) for RHS-1, H = 248.12 mm, B = 149.52 mm, and t = 6.53 mm; and (b) for RHS-2, H = 247.62 mm, B = 149.44 mm, and t = 6.53 mm.

Two longitudinal coupons were cut from the webs of the tubes and tested under tension to determine the steel properties. The average yield strength f_y, the ultimate strength f_u, and the modulus of elasticity were 373 MPa, 510 MPa, and 192.5 GPa, respectively. Poisson´s ratio ν was taken as 0.3. Two six-meter-long RHS beam specimens, simply supported on two rigid steel beams, were subjected to bending tests under four-point loading method. The concentrated transversal forces P were applied at a distance from the nearest support of one-third of the clear span. The load was applied by a 1500 kN capacity MTS hydraulic actuator through a rigid I-section steel beam. At the rigid steel beam supports, a steel roller of 50 mm in diameter and 150 mm in length was symmetrically positioned on a 150×150 mm square, 20 mm thick, steel plate. A load cell was used to monitor the MTS system load. In order to observe the deformation of the specimens, strain gauges (SG) were installed on the steel surfaces of the mid-span section and displacement transducers (DT) were installed at the mid-span section and at the applied load sections. Figure 2 illustrates the test setup scheme.

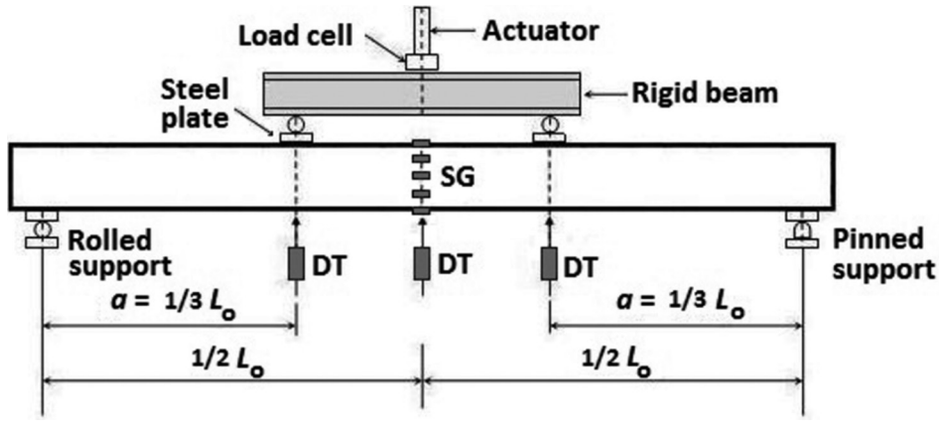

Figure 2
Schematic diagram of test setup.

3. Numerical modeling

3.1 Overview

The finite element analysis commercial software ABAQUS, (SIMULIA, 2011) was used to conduct a numerical, non-linear static analysis of the flexural behavior of RHS beams under four-point load bending. The FE model was initially verified against the experimental results. Detailed information on the model validation may be found in Flor (2018). A parametric study was conducted on the flexural behavior of RHS beams using the validated FE model to investigate the effect of concentrated transversal forces on the bending moment resistance of RHS beams by varying the modes of application of the forces and the corner radius between the flanges and the webs of the RHS steel profile. The study was based on a standard RHS beam with the following parameters: H = 250 mm, B = 150 mm, t = 6.4 mm, L_o = 6000 mm, f_y = 300 MPa, E = 200 GPa and four-point loading method.

3.2 Material modeling

A tri-linear material constitutive model for structural steel was used to describe the idealized uniaxial stress-strain relationship of steel, as shown schematically in Figure 3. The deformation of steel includes a linear elastic phase from zero to the yield strain ε_y at which the plastic behavior of the steel initiates. The plastic behavior that corresponds to the yield of the steel was slightly modified to resolve eventual convergence difficulties during numerical processing. Within the deformation range from the yield strain ε_y to a strain equal to 10 times the yield strain of the steel, $10\varepsilon_y$, the stress linearly increases up to 1.01 fy. By the end of plastic phase, i.e., beyond deformation of $10\varepsilon_y$, a strain hardening stage was considered. Within this phase, stress linearly increases up to the ultimate strength of steel fu. A maximum deformation of $100\varepsilon_y$ reached at fracture was assumed. The von-Mises yield function with associated plastic flow was used in the multiaxial stress states. The steel was also assumed to have isotropic hardening behavior, i.e., the yield surface changes uniformly in all directions when plastic straining occurs.

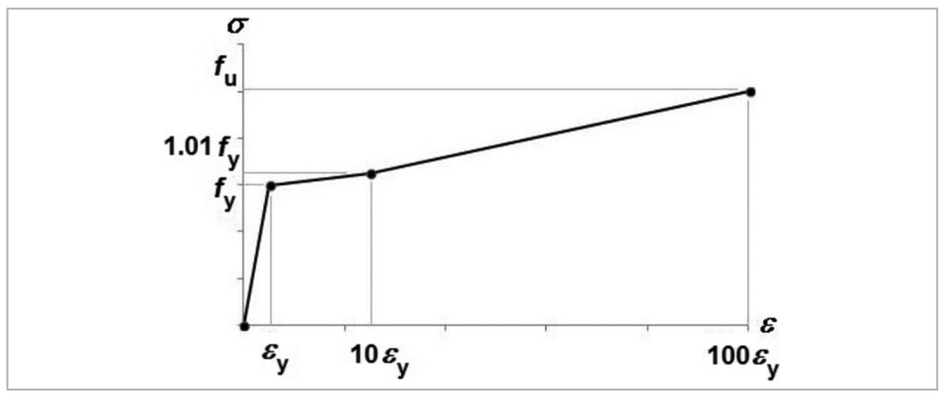

Figure 3
Stress-strain relationship for steel.

3.3 Finite element type and mesh

In order to model the steel tube, a quadrangular first-order (4 nodes) reduced-integration shell element, identified as S4R was selected from theABAQUS element library. Each node has 6 degrees of freedom: 3 translations and 3 rotations. A mesh sensitivity analysis was performed to define an appropriate mesh for the shell elements that provides both accurate results and less computational time. Analyses were conducted using three different seed sizes: 5 mm, 20 mm and 30 mm, in both longitudinal and transversal directions. Additionally, the local mesh near the curved corners was refined in the transversal direction. The transition mesh in each corner used 20, 4 and 3 seeds along the perimeter for models with seed size of 5 mm, 20 mm and 30 mm, respectively. The numerical results for the bending moment resistance were compared to the experimental results. The experimental and numerical comparison showed to be in good agreement. Moreover, there was no significant change in the numerical result among the models. Therefore, a mesh size of 20×20 mm was considered suitable and selected for the proposed numerical study.

3.4 Boundary conditions

For economy of computational resources and efficiency of analysis, the numerical model was developed taking advantage of both geometrical and loading symmetries with respect to both the bending plane and to the transversal plane at the mid-span section, which is perpendicular to the bending plane. Therefore, only one quarter of the beam specimen was considered in the simulations.

Support boundary conditions were established within a region located at the bottom flange of the steel tube and using the Type Beam Multi-Point Constraint (MPC), available in the ABAQUS library. This constraint model provides a rigid beam between two nodes to constrain the displacement and rotation at the first node to the displacement and rotation at the second node, corresponding to the presence of a rigid beam between the two nodes. Initially, the mesh node located at the midpoint of the support central line was defined as a reference point. At this point, the translations in the *x* (U1) and *y* (U2) axis directions and the rotation around the *z* axis (UR3) were restrained, simulating a rolled support boundary condition as shown in Figure 4. The orientation the the global coordinate axes system is also illustrated in this figure. In sequence, the MPC type beam constraint was established between the reference point and all nodes around it that were located within a flat surface of 300 mm in length on the bottom flange of the tube, symmetrical to the support central line. Such modeling approach enabled avoiding stress concentrations within the support neighborhood.

At the *xy* transversal plane of symmetry, the translation in the *z* direction (U3), the rotation about the *x* axis (UR1) and the rotation about the *y* axis (UR2) were restrained. At the *yz* longitudinal plane of symmetry, the translation in the *x* direction (U1), the rotation about the *y* axis (UR2) and the rotation about the *z* axis (UR3) were restrained.

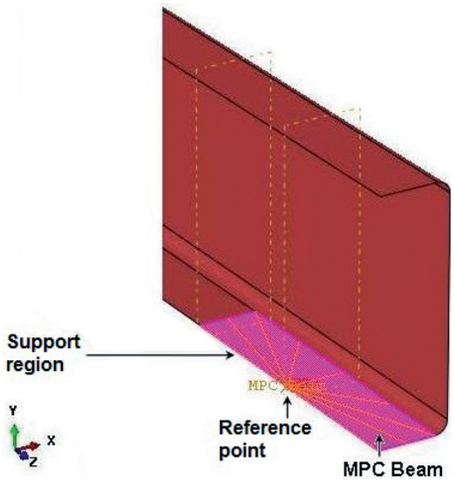

Figure 4
Support boundary conditions.

3.5 Load modeling

Concentrated transversal forces were modeled by using the pressure type of load available in the ABAQUS library, acting perpendicularly over the flat portion of the upper flange of the tubular beam, over a 150-mm-long surface. Two different modes of loading application were numerically investigated. In the first load case (LC1), the load was directly applied to the flat portion of the upper flange of the tubular beam. The second load case (LC2) was similar to LC1, though in the LC2 case, doubler plates of 6.4 mm in thickness and 150 mm in length were installed on the flat portion of both webs. The modeling of the two load cases investigated is illustrated in Figure 5. The 4-node shell element (S4R) was used to model the doubler plates in LC2. The steel-steel interface between the doubler plates and the tube was modeled as a tie interaction around the perimeter of the contact between both surfaces, simulating a fillet weld commonly used in practical situations. For each load case investigated, the influence of the corner radius between the flanges and the webs of the RHS steel profile on the beam moment resistance was examined. Table 2 presents the values of the outer radius r_o, the inner radius r_i and the mean radius r_m considered in this numerical analysis. The cross-sectional dimensions of the steel tube were kept constant.

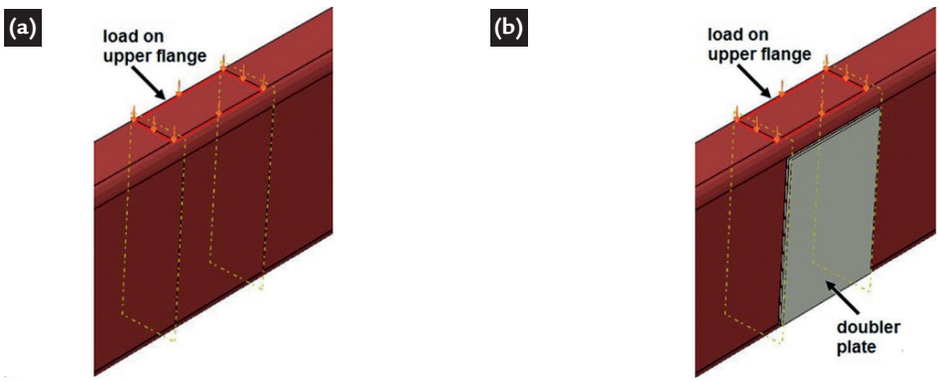

Load case 1 (LC1) Load case 2 (LC2)

Figure 5
Load modeling.

Corner radius			LTB		FLB		WLB	
r_e mm	r_i mm	r_m mm	λ	λ_p	λ	λ_p	λ	λ_p
7.2	0.8	4.0	91.59	95.04	21.19	28,92	36.81	62.48
9.6	3.2	6.4	91.69	95.75	20.44	28.92	36.06	62.48
16.0	9.6	12.8	91.99	97.57	18.44	28.92	34.06	62.48
28.8	22.4	25.6	92.78	100.98	14.44	28.92	30.06	62.48
35.2	28.8	32.0	93.28	102.55	12.44	28.92	28.06	62.48

Table 2
Corner radius and slenderness parameters.

4. Results and discussion

4.1 Slenderness parameters

Table 2 lists λ and λ_p slenderness parameters respective to the bending moment resistance for LTB, FLB and WLB ultimate limit states, calculated according to the Brazilian standard ABNT NBR 8800:2008 (refer to Table 1) using nominal values for steel properties. The values obtained for λ were below λ_p for all values of the corner radius investigated. Therefore, the bending moment resistance is not limited by the occurrence of either lateral-torsional buckling or local buckling in the compression flange or the compression webs.

4.2 Experimental results

The moment-displacement (M-δ) experimental curves obtained for the two full scale RHS beam specimens are shown in Figure 6. The displacement refers to the deflection at the mid-span section. Both RHS specimens had a nominal outer corner radius of 16 mm and behaved in a very similar manner. The real outer corner radius measured prior to the test was 20.1 mm. There is an elastic phase in which a linear relationship response between moment and displacement is observed. This initial phase is followed by an inelastic stage in which there is a gradual degradation in the flexural stiffness up to maximum moment. The post-peak behavior shows the descending portion of the curve. The maximum moment values obtained for RHS-1 and RHS-2 specimens were 147.18 kN·m and 147.61 kN·m, respectively. The predicted value for the plastic moment Mpl was 147.87 kN·m, given by the product of the plastic section modulus Z and the steel yield strength f_y, i.e., $M_{pl} = Z \cdot f_y$. It is worth mentioning that the corner radius was taken into consideration in the hand calculation of the plastic section modulus. By the end of the test, both specimens presented a typical global beam bending associated with a large localized plastic deformation with geometrical folding on the upper flange and with a local plastic deformation of the compressive region of the webs beneath the applied load. It can be observed from Figure 6 that the effect of the concentrated transversal force had negligible influence on the moment resistance of the tubular beam, since the maximum moment obtained in the tests almost reached the theoretical plastic moment. Figure 7a depicts the deformed configuration in neighborhood of the concentrated transversal force section when the applied load reached approximately the maximum load for RH-1 specimen. Figure 7b shows a more pronounced deformed configuration of the same section by the end of the flexural test when a higher level of displacement was reached.

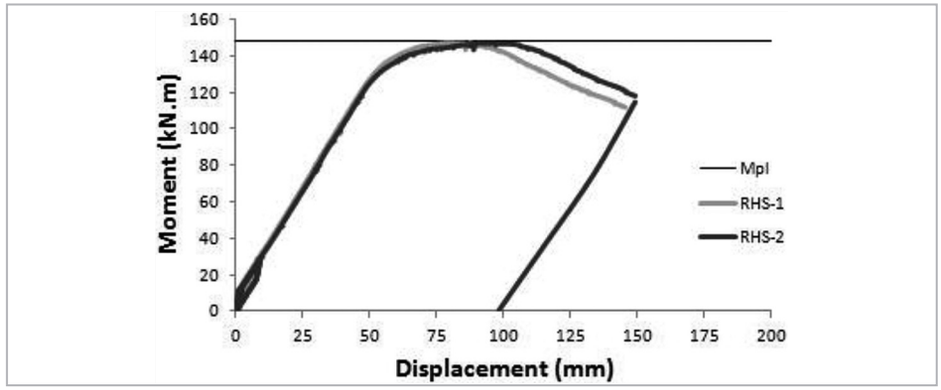

Figure 6
Experimental moment-displacement curves for RHS beam specimens.

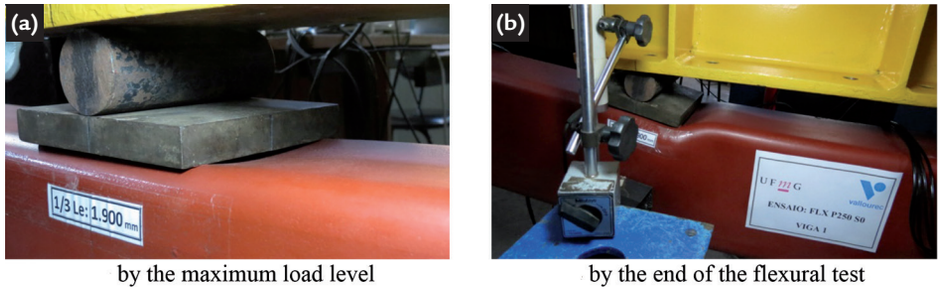

by the maximum load level | by the end of the flexural test

Figure 7
Deformed configuration near the concentrated transversal force section.

4.3 Numerical results

Figures 8 to 12 show the moment-displacement (M-δ) curves obtained from the numerical analyses carried out for the FE models considering each of the five different values for the mean corner radius. In each figure, the moment-displacement curves corresponding to each of the two load cases under investigation are plotted. The theoretical value of the plastic moment is also plotted in the graphs as the horizontal line. It is clearly observed that all curves corresponding to LC1, in which the load is applied directly on the flat part of the upper flange of the tube, do not reach the plastic moment and present a post-peak descending portion. In this case, it is evident that failure by concentrated force prevented the full development of the cross sectional moment resistance. Applying the load directly on the upper flange and strengthening the flat portion of the webs with doubler plates at the applied load section (LC2), the flexural behavior of the beams improves significantly. However, for cross-sections with larger corner radii (25.6 mm and 32 mm), the performance still remains below the plastic moment. Figure 13 demonstrates the deformed configuration in the neighborhood of the concentrated force observed for the numerical simulation performed for a cross-section with mean radius of 12.8 mm and load applied as LC1, which corroborates the experimental results. When doubler plates were used, no deformed configuration was noticed on either the upper flange or the webs.

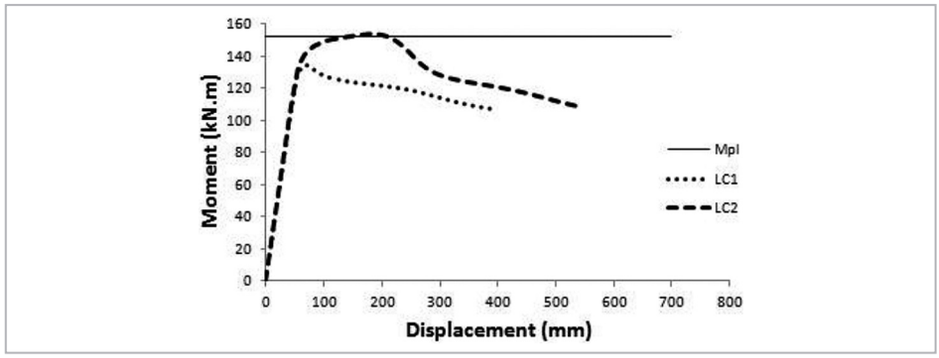

Figure 8
Numerical M-δ curve (r_m=4 mm).

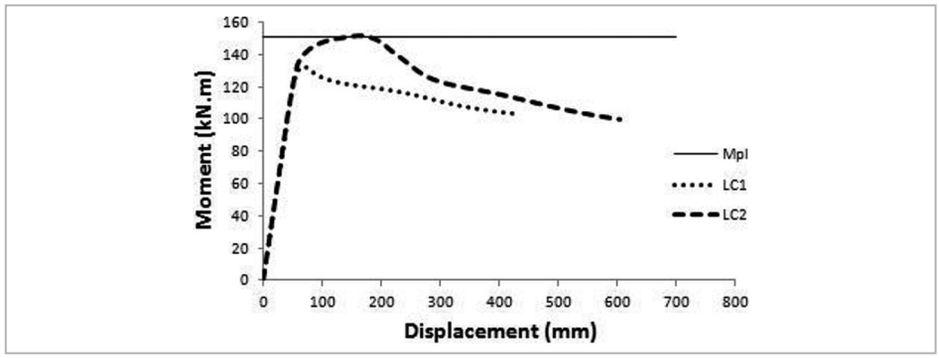

Figure 9
Numerical M-δ curve (r_m=6.4 mm).

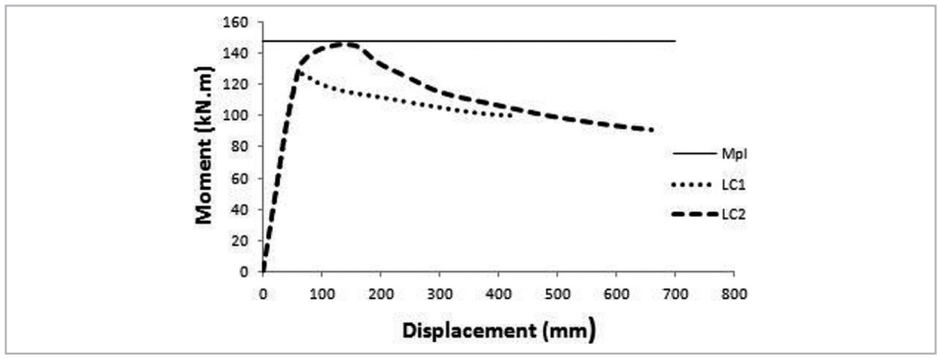

Figure 10
Numerical M-δ curve (r_m=12.8 mm).

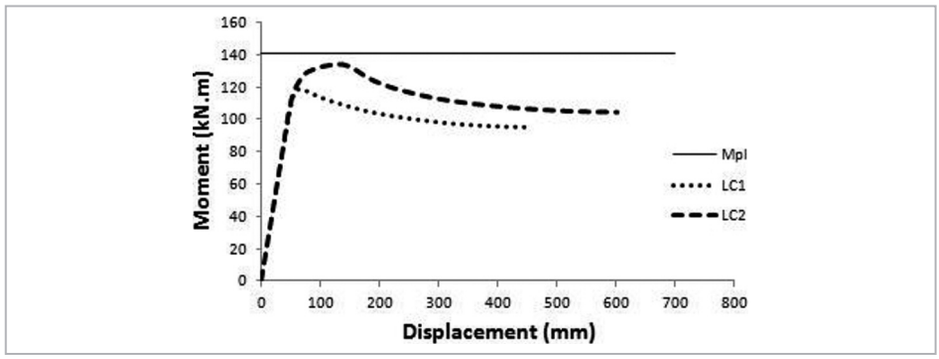

Figure 11
Numerical M-δ curve (r_m=25.6 mm).

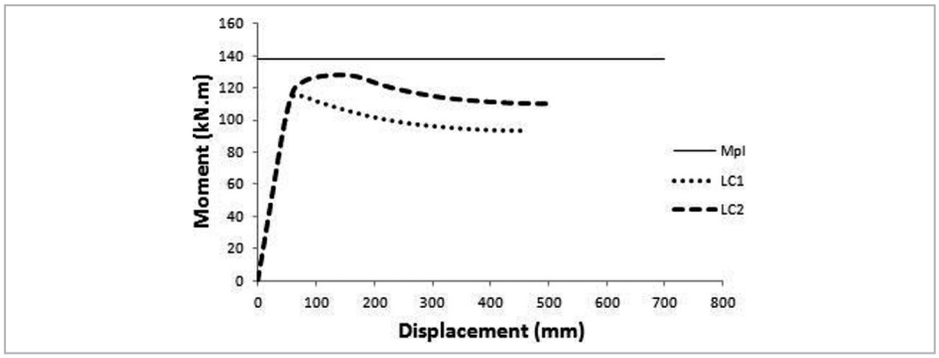

Figure 12
Numerical *M*-δ curve (r_m=32 mm).

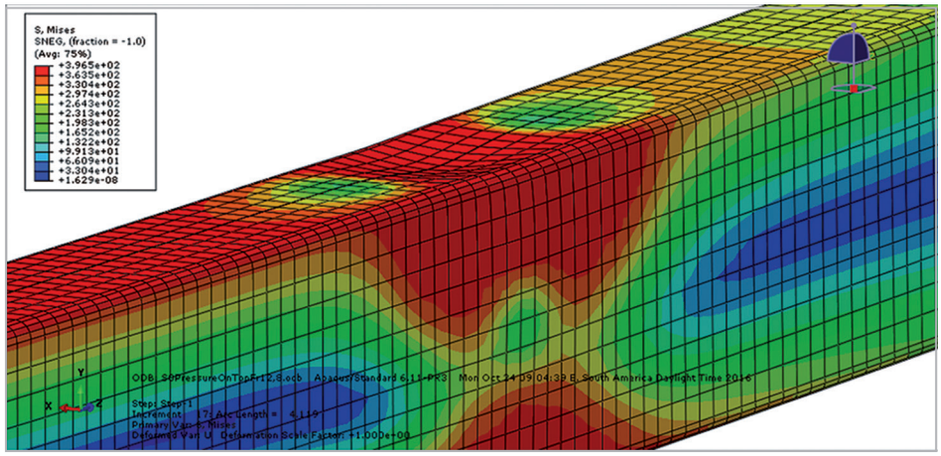

Figure 13
FE model with localized deformation.

Table 3 summarizes the results obtained for the maximum moment for the five different values of the mean corner radius r_m considered in this investigation. In this table, M_1 denotes the numerical bending moment resistance obtained from modeling the applied load according to the first load case (LC1), M_2 denotes the numerical bending moment resistance obtained from modeling the applied load according to the second load case (LC2) and M_{Rk} denotes the theoretically estimated bending moment resistance.

Observing the results obtained for the M_1/M_{Rk} ratio, it is verified that the effect of the concentrated force is quite significant when load is applied directly to the upper flange of the rectangular steel tube. Furthermore, the larger the corner radius, the more detrimental the effect of the concentrated transversal force, keeping the cross-sectionalmajor dimensions unchanged (i.e., H = 250 mm, B = 150 mm and t = 6.4 mm). For the smallest radius investigated (4 mm), the reduction was 11.5% while for the largest radius (32 mm) the decrease was 16%. For the tested specimens with mean radius of 12.8 mm, the reduction was almost 14%. The results obtained for the M_2/M_{Rk} ratio showed that it is possible to minimize the deleterious effect of the concentrated force by installing doubler plates on the webs of the RHS profile. On average, the reduction on the moment resistance was 2.4%. It is noted, however, that this decrease was more pronounced in the sections with larger radii. For the largest radius investigated (32 mm), the reduction was 7%. It is important to mention that the European standard EN 10219-2: 2006 for cold-formed tubes limits the outer and inner corner radii of rectangular steel hollow sections in function of the tube wall thickness. These provisions are very pertinent, since they allow avoiding the manufacture of rectangular tubes with high-value corner radii, which could potentiate the negative influence of the concentrated force on the bending moment resistance of hollow steel section beams.

		LC1		LC2	
r_m	M_{Rk}	M_1	M_1/M_{Rk}	M_2	M_2/M_{Rk}
mm	kN·m	kN·m		kN·m	
4.0	152.36	134.82	0.885	153.54	1.008
6.4	151.15	132.72	0.878	151.50	1.002
12.8	147.87	127.33	0.861	146.26	0.989
25.6	141.15	118.71	0.841	134.23	0.951
32.0	137.70	115.68	0.840	128.09	0.930
Mean			0.861		0.976
Standard deviation			0.021		0.034

Table 3
Summary of numerical results for moment resistance.

5. Conclusions

This paper has investigated the effect of concentrated transversal forces on the moment resistance of rectangular hollow steel section (RHS) beams. As expected, it was observed that rectangular tubular steel sections may fail by localized plastic deformations beneath the applied load, whenever this load causes compression to the webs.

It was also noted that the bending moment resistance given by the plastic moment can be significantly reduced by the effect of the concentrated transversal force when rectangular tubes with corner radius superior to the specified values by the European standard EN 10219- 2: 2006 are employed. The installation of doubler plates along the flat part of the webs of the RSH profile at the applied load section can reduce or even eliminate the detrimental effect of the concentrated transversal force on the moment resistance. Finally, it is important to mention that several studies are still necessary to fully examine the broad range of situations in order to develop safe and accurate design procedures that take into account the effects of concentrated force on RHS beams. Parameters such as cross-sectional dimensions, mechanical properties of the structural steel, locations of the applied loads, applying length, within others, still require further investigations.

Acknowledgements

The authors are grateful to Vallourec Tubos do Brasil S.A., for providing the steel tubes in the experimental program of this research project. The financial support of the National Council for Scientific and Technological Development (CNPq) and the Foundation for Research Support of Minas Gerais (FAPEMIG) are acknowledged.

References

ARAÚJO, A. H. M., SARMANHO, A. M., BATISTA, E. M., REQUENA, J. A. V., FAKURY, R. H., PIMENTA, R. J. ***Projeto de estruturas de edificações com perfis tubulares de aço.*** Belo Horizonte: Ed. do autor, 2016. 598p.

ASSOCIAÇÃO BRASILEIRA DE NORMAS TÉCNICAS. ABNT NBR 8800:2008. Projeto de estruturas de aço e de estruturas mistas de aço e concreto de edifícios. Rio de Janeiro, 2008.

CARTER, C. J. ***Stiffening of wide-flange columns at moment connections: wind and seismic applications.*** Chicago, IL: American Institute of Steel Construction, 1999. (Steel Design Guide 13).

ELGAALY, M. Web design under compressive edge loads. ***Engineering Journal, AISC,*** v. 20, n. 4, p. 153–171, 4th Quarter, 1983.

ELGAALY, M., SALKAR, R. Web crippling under edge loading, In: PROCEEDINGS OF AISC NATIONAL STEEL CONSTRUCTION CONFERENCE, Washington, DC, 1991.

EUROPEAN COMMITTEE FOR STANDARDIZATION. EN 10219-2:2006. Cold formed welded structural hollow sections of non-alloy and fine grain steels. Part2: Tolerances, dimensions and sectional properties. Brussels, 2006.

FLOR, J. M. ***Estudo experimental e numérico de vigas mistas constituídas de perfil de aço tubular retangular preenchido com concreto autoadensável em escala real.*** Belo Horizonte: Universidade Federal de Minas Gerais, 2018. (Doctoral Dissertation - Unpublished).

GRAHAM, J. D., SHERBOURNE, A. N., KHABBAZ, R. N. ***Welded interior beam-to-column connections.*** Chicago, IL: American Institute of Steel Construction, 1959.

GRAHAM, J. D., SHERBOURNE, A. N., KHABBAZ, R. N., JENSEN, C. D. Welded interior beam-to-column connections. ***Welding Research Council,*** n. 63, p. 1-28, 1960. (Bulletin).

HAJJAR, J. F., DEXTER, R. J., OJARD, S. D., YE, Y., COTTON, S. C. Continuity plate detailing for steel moment-resisting connections. ***Engineering Journal, AISC,*** v. 40, n. 4, p. 189-211, 4th Quarter, 2003.

PROCHNOW, S. D., YE, Y., DEXTER, R. J., HAJJAR, J. F, COTTON, S. C. Local flange bending and local web yielding limit states in steel moment resisting connections. In: LEON, R. T., EASTERLING, W. S. (Eds.). ***Connections in Steel Structures IV - Behavior, Strength and Design.*** Chicago, IL: American Institute of Steel Construction, 2000. p. 318–328.

ROBERTS, T. M. Slender plate girders subjected to edge loading. In: PROCEEDINGS OF THE INSTITUTION OF CIVIL ENGINEERS. Part 2, v. 71, n. 3, p. 805-819, September,1981.

SHERBOURNE, A. N., JENSEN, C. D. ***Direct welded beam column connections,***

Bethlehem, PA: Fritz Engineering Laboratory, Lehigh University, 1957. (Report n. 233.12).

SIMULIA, DassautSystèmes Corp. Abaqus Documentation, v. 6.11, Providence, RI, USA, 2011.

SUMMERS, P. A., YURA, J. A. ***The behavior of beams subjected to concentrated loads.*** Austin, TX: Phil M. Ferguson Structural Engineering Laboratory, University of Texas, August, 1982. (Report n. 82-5).

TROUP, E. W. Effective contract and shop drawings for structural steel. In: PROCEEDINGS OF THE AISC NATIONAL STEEL CONSTRUCTION CONFERENCE, 1999, Toronto. ***Anais...***American Institute of Steel Construction, Chicago, IL,p.37-1--37-15, 1999.

Received: 9 August 2018 - Accepted: 23 April 2019.